Simulation of Ostwald Ripening in a Reactive Batch Crystallizer

N. S. Tavare
Department of Chemical Engineering
University of Manchester
Institute of Science & Technology
Manchester, M60 1QD England

Introduction

The structure of a precipitate, comprising mainly the crystal size distribution, morphology, lattice and surface structure, and nature of interparticle interaction resulting from agglomeration processes, is the result of many kinetic events that interact with each other. The process of particle coarsening by Ostwald ripening or aging—i.e., the growth of large crystals at the expense of small ones that dissolve and finally disappear completely—is important in many precipitation systems and yields narrower product, leading eventually toward equilibrium with a minimum total surface free energy. Numerous theoretical and experimental studies using some simplified assumptions have appeared in the crystallization literature (Hanitzsch and Kahlweit, 1969; Dunning, 1973; Kahlweit, 1975; Wey and Strong, 1977; Sugimato, 1978; Venzl, 1983; Matz, 1984; Brakalov, 1985). Usually the solubility in the driving force to the kinetic event will change with particle size, as given by the Gibbs-Thomson relation, which for the present purpose may be written as

$$c_L^* = c^* \exp\left(\frac{\Gamma_D}{L}\right) \tag{1}$$

where

$$\Gamma_D = \frac{4\sigma v}{RT} \tag{2}$$

The critical size L^*, above which a crystal grows with a certain size-dependent growth rate and below which it dissolves, may be determined as

$$L^* = \frac{\Gamma_D}{\ln\left(\frac{c_b}{c^*}\right)} \tag{3}$$

At least three kinetic events should appear in any simulation according to their significance and importance. At any time, nucleation at L^*, growth of crystals above L^*, and dissolution below L^* may be assumed to occur simultaneously, the respective rates being determined from the kinetic expressions at prevailing operating conditions. The agglomeration processes are generally associated with precipitate formation but will not be considered in the present investigation. Normally a homogeneous reaction between two reacting components precedes the precipitation step. Thus the purpose of this note is to attempt to simulate and characterize the reactive precipitation process exhibiting Ostwald ripening in a perfectly mixed batch crystallizer configuration.

Theory

For the present purpose two reactant species, A and B, mix perfectly and then react together homogeneously in a batch crystallizer with first-order reaction kinetics with respect to each of the reactive components as follows:

$$A + B \rightarrow C$$
$$r_C = k c_A c_B \tag{4}$$

Precipitation of the solid product C resulting from this liquid phase reaction occurs simultaneously because the fluid phase becomes supersaturated with respect to component C. Conventional power law growth kinetics incorporating the Gibbs-Thomson solubility relation for crystals larger than L^*:

$$G = k_g(c - c_L^*)^g = k_g[c - c^* \exp(\Gamma_D/L)]^g \tag{5}$$

and dissolution kinetics for crystals smaller than L^*:

$$D = k_d(c_L^* - c)^d = k_d[c^* \exp(\Gamma_D/L) - c]^d \tag{6}$$

are used. Note that the units of concentration used are mol/kg. Nuclei are produced at L^* and the nucleation kinetics may be

expressed by

$$B_n = k_b(c - c^*)^b \tag{7}$$

The concentration profiles with time for the limiting reactant A, species B, and product C in a constant-volume batch crystallizer may be written as

$$\frac{dc_A}{dt} = - kc_Ac_B \tag{8}$$

$$\frac{dc_B}{dt} = kc_Ac_B \tag{9}$$

$$\frac{dc_C}{dt} = - kc_Ac_B - \alpha_c \tag{10}$$

where

$$\alpha_C = k_v\rho_c(3A_1 + B_nL^{*3}) \tag{11}$$

the boundary conditions being

$$c_A = \bar{c}_{A_o}, \quad c_B = \bar{c}_{B_o}, \quad c_C = 0 \text{ at } t = 0 \tag{12}$$

The population balance equation for such a batch crystallizer configuration with negligible agglomeration and attrition is

$$\frac{\partial n}{dt} + \frac{\partial nG}{\partial L} = 0 \quad L_m > L > L^*$$

$$\frac{\partial n}{\partial t} + \frac{\partial nD}{\partial L} = 0 \quad L^* > L > L_o \tag{13}$$

If the crystals are generated at $L = L^*$ by nucleation at a rate B_n and disappear at $L = 0$ by dissolution at a rate B_D, the moment transformation of population balance, eq. 13, with respect to size is written as

$$\frac{dN}{dt} = B_n\delta(L - L^*) - B_D\delta(L) \tag{14}$$

$$\frac{dL}{dt} = N_1 + B_nL^* \tag{15}$$

$$\frac{dA}{dt} = 2L_1 + B_nL^{*2} \tag{16}$$

$$\frac{dW}{dt} = k_v\rho_c\left(3\frac{A_1}{k_a} + B_nL^{*3}\right) \tag{17}$$

where

$$N_1 = \int_{L_o}^{L^*} nDdL + \int_{L^*}^{L_m} nGdL \tag{18}$$

$$L_1 = \int_{L_o}^{L^*} nDLdL + \int_{L^*}^{L_m} nGLdL \tag{19}$$

$$A_1 = k_a\int_{L_o}^{L^*} nDL^2dL + k_a\int_{L^*}^{L_m} nGL^2dL \tag{20}$$

with boundary conditions

$$N = L = A = W = 0 \quad \text{at} \quad t = 0 \tag{21}$$

The size of the largest probable particle may be determined by

$$\frac{dL_m}{dt} = G(L_m) \tag{22}$$

Computational Aspects

In order to evaluate the performance characteristics of the reactive batch precipitator, the set of equations described above was solved simultaneously for the specific parameters listed in Table 1. Initially, one reaction occurs in the batch unit until the concentration of the product C reaches the saturation point. As soon as the solution becomes supersaturated with respect to C, nucleation and subsequent evolution of crystal size distribution via growth and dissolution commences. Consequently only the differential equations describing the concentration profiles, Eqs. 8–10, are integrated initially (α_C having been set equal to zero) until the concentration of C in the liquid phase reaches the saturation concentration. Once the reaction mixture becomes supersaturated with respect of C, the set of eight differential equations, Eqs. 8–10, 14–17, and 22, along with the partial differential equation representing the population balance, Eq. 13, is solved simultaneously.

All the differential equations involved were integrated by the fourth-order Runge-Kutta method with an integration step length of $\Delta t = 1$ s using the appropriate initial conditions, Eqs. 12 and 21, and the integrals in Eqs. 18–20 evaluated by the simple Euler's formula with a specified size step length (0.0125 μm). The partial differential equation, Eq. 13, was solved by a modified method of numerical integration along the characteristics with a specified grid length of size. In the algorithm all the differential equations—Eqs. 8–10, 14–17, and 22—were initially integrated with a step length of $\Delta t = 1$ s until the increment in size of the largest crystal as found by Eq. 22 was equal to the crystal size grid length of 0.0125 μm used in the solution of the partial differential equation. A representation of typical grids at any times t and $t + \Delta t_1$ is depicted in Figure 1, Δt_1 being

Table 1. Parameters Used in Calculations

M_C	100
c_C^*, mol/kg	0.1
c_{A_o}, mol/kg	1
c_{B_o}, mol/kg	1
V, kg	200
ρ_c, kg/m^3	2,000
Γ_D, m	2×10^{-7}
k_a	3.68
k_v	0.52
τ, s	10,000
k, kg/mol · s	0.1
g	1.5
k_g, m/[s(mol/kg)^g]	7.9×10^{-8}
b	4.5
k_b, no/[kg · s(mol/kg)^b]	3.1×10^{10}
d	1.5
k_d, m/[s(mol/kg)^d]	7.9×10^{-8}
β	1

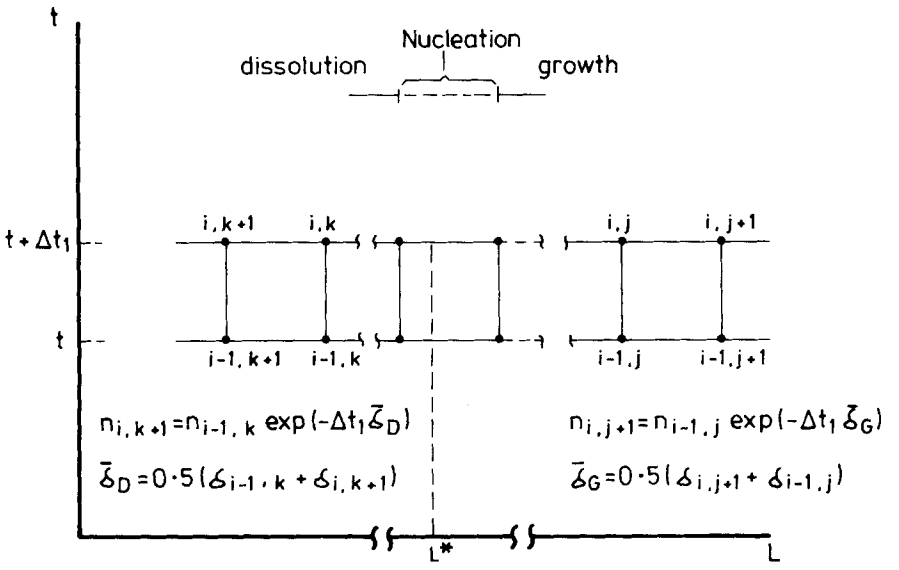

Figure 1. Representation of grids at any time for numerical solution.

the time required to grow the largest crystal by a step length in size (0.0125 μm). Nuclei population density, evaluated as

$$n(t, L^*) = B_n \frac{\Delta t_1}{\Delta L} \tag{23}$$

was assigned to the grid corresponding to the critical size L^* as defined by Eq. 3. The disappearance rate, B_D, was defined as the product of the population density and the dissolution rate at the end of the first grid. The probable maximum size in the distribution was determined by following the largest size found by Eq. 22 either of the crystal nucleated at zero time or of any other nuclei having larger size. The minimum size was also followed in order to monitor the progress of the dissolution from the smallest of either dissolving crystal or nuclei generated. Sometimes if the time step length of $\Delta t = 1$ was too large and produced a size increment greater than 0.0125 μm, a provision to reduce the step length Δt proportionately for the integration step was incorporated in the algorithm so as to keep the size increment below one size grid length.

Results and Discussion

The results of calculations depicting the concentration of A, and of C in the solution, c_A and c_C, respectively, and in the solid phase—i.e., the magma density M_T as a function of time—in a batch crystallizer are reported in Figure 2. Initially (up to 300 s), the concentration of A decreases rapidly with a corresponding increase in concentration of C in the liquid phase due to high reaction rate, and then slowly later. As the reaction proceeds with time the reaction mixture will become saturated first and then supersaturated with respect to C, causing the production of a solid phase. The concentration of C passes through the maximum and remains near saturation later. Molal magma concentration increases rapidly and then remains constant. Magma

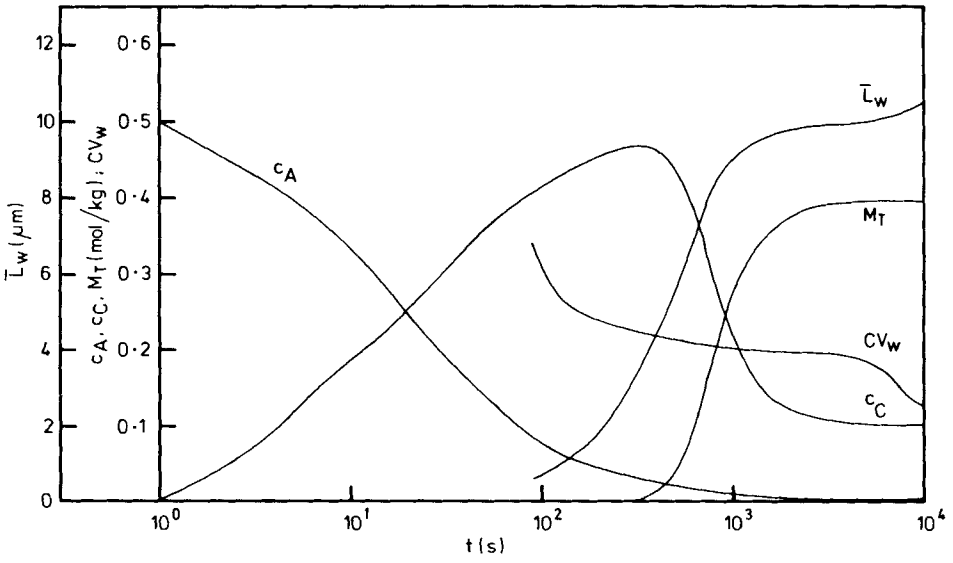

Figure 2. Profiles with time for concentrations and statistics of product crystals.

Table 2. Effect of Ratio of Dissolution to Growth Rates on Performance Characteristics at the End of Batch Time

β	$c_A \times 10^4$ mol/kg	c_C mol/kg	M_T mol/kg	$\bar{L}_w$ μm	CV_w %	$N \times 10^{-12}$ no/kg
1	9.98	0.1026	0.396	10.51	12.95	3.83
2	9.97	0.1027	0.396	10.49	13.20	3.20
5	9.97	0.1027	0.396	10.41	13.90	3.40
10	9.97	0.1027	0.396	10.31	14.82	3.15
0	9.98	0.1006	0.398	7.82	19.7	12.05

densities determined from the solution concentration difference and calculated from Eq. 17 were identical. Also included in Figure 2 are the time variations of the statistics of the solid product C (i.e., weight mean size and coefficient of variation). Initially, weight mean size increases rapidly, and then only slightly; the coefficient of variation decreases with time. Thus particle coarsening with a reduction in the coefficient of variation occurs during the aging process.

Keeping all other parameters in Table 1 and kinetic relations constant, the parameter β representing the ratio of dissolution to growth rates was varied over the range from 0 to 10; the results are reported in Table 2. With an increase in β there is only a slight change in statistics of the solid product C for the present configuration. Also included in Table 2 are the corresponding results for a reactive precipitation system without the Ostwald ripening effect ($\beta = 0$). The product characteristics for this case are different.

The calculated population density curves as a function of crystal size obtained by solving the population balance equation, Eq. 13, at two times are reported in Figure 3. Corresponding population density curves for the reactive precipitation system without the Ostwald ripening effect at the same two times are also included in Figure 3. The widely varying size distributions and their corresponding statistics, Figure 3, are a consequence of the different kinetic events reflected in different supersaturation profiles in a batch crystallizer.

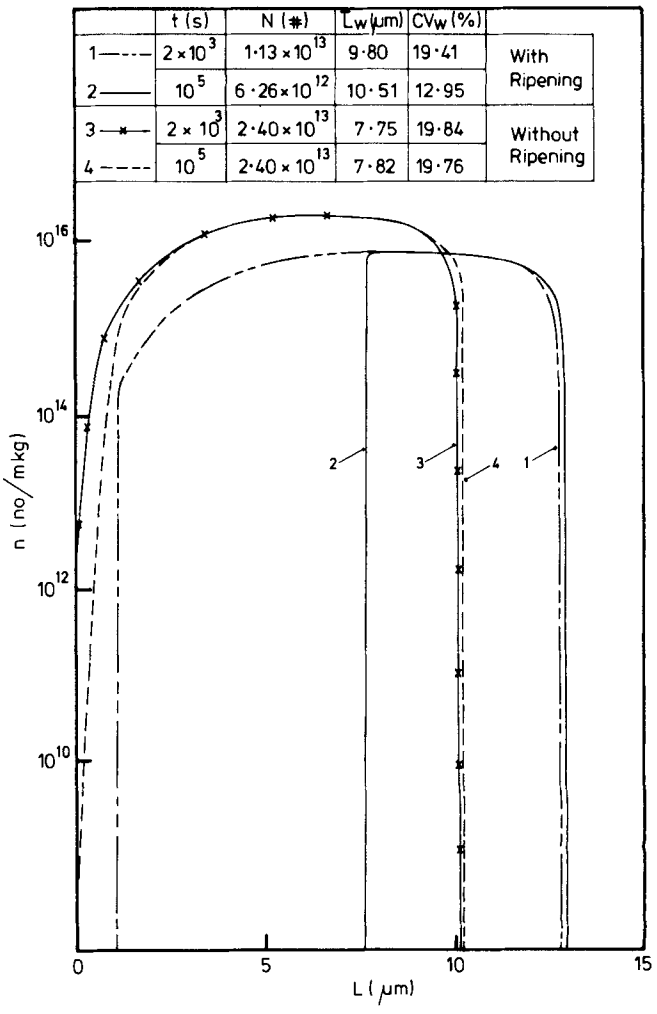

Figure 3. Population density plots: effect of Ostwald ripening.

Notation

A = total surface area, m^2/kg
A_1 = modified surface area, Eq. 20, $m^3/s \cdot kg$
b = nucleation order
B_D = disappearance rate per grid, no/s · kg · m
B_n = nucleation rate, no/s · kg; nucleation rate per grid, no/s · kg · m
c = concentration, mol/kg
c^* = saturation concentration of a large crystal with flat surface, mol/kg
CV = coefficient of variation, %
d = dissolution order
D = overall linear dissolution rate, m/s
g = growth rate order
G = overall linear growth rate, m/s
k = reaction rate coefficient, kg/mol · s
k_a = area shape factor
k_b = nucleation rate coefficient, no/[sk · kg(mol/kg)^b]
k_d = dissolution rate coefficient, m/[s(mol/kg)^d]
k_g = growth rate coefficient, m/[s(mol/kg)^g]
k_v = volume shape factor
L = crystal size, total length, μm, m, m/kg
L_1 = modified total length, Eq. 19, $m^2/s \cdot kg$
L^* = Gibbs-Thomson critical size, Eq. 3, m
ΔL = size step length, m
M_C = molecular weight of component C
M_T = molal magma density, mol/kg
n = population density, no/m · kg
N = total number of crystals, no/kg
N_1 = modified number of crystals, Eq. 18, no · m/s · kg
r_C = reaction rate, mol/s · kg
R = universal gas constant, J/mol · K
t = time, s
Δt, Δt_1 = step lengths, s
T = temperature, K
v = molecular volume of solute, m^3/mol
V = solvent capacity, kg
W = crystal molal mass, mol/kg

Greek letters

α = solid deposition rate, mol/kg · s
β = ratio of dissolution to growth rate, $= D/G$
Γ_D = capillary constant from Gibbs-Thomson equation, Eq. 2, m
δ = $\partial G/\partial L$, 1/s; delta Dirac function
ρ_c = crystal density, kg/m^3
σ = surface energy, J/m^2
τ = batch run time, s

Subscripts

A, B, C = components
b = bulk
D = dissolution
G = growth
i, j, k = index variables
L = at size L

m = maximum, upper
o = initial, lower
w = weight basis

Superscripts

$*$ = equilibrium
$-$ = average

Literature cited

Brakalov, L. B., "On the Mechanism of Magnesium Hydroxide Ripening," *Chem. Eng. Sci.*, **40**(2), 305 (1985).

Dunning, W. J., "Ripening and Aging Processes in Precipitates, *Particle Growth in Suspensions*, L. Smith, ed., SCI Monog. **38**, 3 (1973).

Hanitzsch, E., and M. Kahlweit, "Aging of Precipitates, *Industrial Crystallization, Symp. Proc.*, Inst. Chem. Eng., London, 130 (1969).

Kahlweit, M., "Ostwald Ripening of Precipitates," *Adv. Colloid. Interface Sci.*, **5**, 1 (1975).

Matz, G., "Crystallization Processes," *Industrial Crystallization 84*, S. J. Jancic, and E. J. de Jong, eds., Elsevier, Amsterdam, 103 (1984).

Sugimato, T., "General Kinetics of Ostwald Ripening of Precipitates," *J. Colloid. Interface Sci.*, **13**, 161 (1978).

Venzl, G., "Ostwald Ripening of Precipitates. I: Numerical Solution for the Particle Size Distribution Function in Closed Systems," *Ber. Bensenges. Phy. Chem.*, **87**, 318 (1983).

Wey, J. S., and R. W. Strong, "Influence of the Gibbs-Thomson Effect on the Growth Behavior of AgBr Crystals," *Photographic Sci. Eng.* **21**(5), 248 (1977).

Manuscript received Feb. 7, 1986, and revision received May 21, 1986.